Journal of Luminescence 135 (2013) 178–186

Contents lists available at SciVerse ScienceDirect

Journal of Luminescence

journal homepage: www.elsevier.com/locate/jlumin

Review

Spectroscopic properties of Er:NaLa$(WO_4)_2$ crystals and effect of Ce codoping onto the excited state energy transformation in this crystal

L. Bonelli [a], F. Cornacchia [a], M. Tonelli [a], D.A. Lis [b,*], K.A. Subbotin [b], V.A. Smirnov [b], E.V. Zharikov [c]

[a] NEST-INFM-CNR-Dipartimento di Fisica dell'Universit'a di Pisa, Largo B. Pontecorvo 3, 56127 Pisa, Italy
[b] A.M. Prokhorov General Physics Institute of Russian Academy of Science, Vavilova street 38, Moscow 119991, Russia
[c] D.I. Mendeleyev University of Chemical Technology of Russia, Miusskaya Sq. 9, Moscow 125047, Russia

ARTICLE INFO

Article history:
Received 25 April 2012
Received in revised form
22 August 2012
Accepted 27 August 2012
Available online 10 October 2012

Keywords:
Tungstate
Er-doped
Ce-doped
Energy transfer

ABSTRACT

We report on the spectroscopic investigation of Erbium and Cerium co-doped Czochralski-grown NaLa$(WO_4)_2$ crystals. We measured the Er energy levels positions and calculated the Judd–Ofelt parameters as well as the radiative lifetimes and branching ratios for the transitions under investigation. The dynamics of population of the $^4S_{3/2}$, $^4I_{11/2}$ and $^4I_{13/2}$ multiplets of Er^{3+} was analyzed in order to determine the influence of the energy transfer mechanism Er–Ce onto the 1.5 μm emission. The results of Er room temperature lifetimes measurements show that the $^4I_{11/2}$ lifetime reduces significantly as the Ce concentration increases, starting from 183 μs for the 0.4 at% Er doped sample to 15 μs for the 16% Ce-codoped crystal. On the contrary, the lifetime of $^4I_{13/2}$ Er state reduces simultaneously of only about 10%. The obtained results suggest the possibility to obtain efficient 1.5 μm laser emission from NaLa$(WO_4)_2$.

© 2012 Elsevier B.V. All rights reserved.

Contents

1. Introduction

Er^{3+} ion, due to its energy level structure, is a very useful and attractive activator for several laser applications. The main transitions are the $^4S_{3/2} \rightarrow {}^4I_{15/2}$ around 550 nm, the $^4I_{11/2} \rightarrow {}^4I_{13/2}$ around 3 μm and the $^4I_{13/2} \rightarrow {}^4I_{15/2}$ around 1.5 μm. The visible transition results applicable in color display technology, optical data storage and undersea communication [1,2]. The 3 μm laser emission has medical application. The most interesting is the 1.5 μm transition that can be useful to develop optical communication devices [3,4,5]. Many host crystals and different pump sources have been used to demonstrate the Er^{3+} laser action near 1.5 μm at various temperatures [6–12].

One of the limiting factors in the use of Er^{3+} as the active ion of efficient 1.5 μm laser sources, pumped by standard InGaAs laser diodes at $\lambda = 970$ nm, is too slow excited state energy

* Corresponding author. Tel.: +7 499 5038374.
E-mail address: lisdenis@mail.ru (D.A. Lis).

0022-2313/$ - see front matter © 2012 Elsevier B.V. All rights reserved.
http://dx.doi.org/10.1016/j.jlumin.2012.08.055

transfer from the diode pumped manifold $^4I_{11/2}$ onto the upper laser level $^4I_{13/2}$. The excited state energy linger at the $^4I_{11/2}$ excited state and due to the competing up-conversion processes like ($^4I_{11/2}$, $^4I_{11/2}$)→($^4I_{15/2}$, $^4S_{3/2}$) transfers into the higher-lying excited state $^4S_{3/2}$, which, in turn, depopulates by green fluorescence (transition $^4S_{3/2}\rightarrow{}^4I_{15/2}$).

In order to improve the efficiency of the Er^{3+} emission near 1.5 μm it is very important, to enhance the transfer rate from $^4I_{11/2}$ to $^4I_{13/2}$. A possible solution relies in the introduction of another co-doping rare earth ion that increases the upper laser level population through energy transfer mechanisms with Er^{3+}. The use of Ce as such co-doping ion has been yet investigated in several vitreous [12,13], and crystalline [10,14–17] materials. In particular, the substantial enhancement of 1.55 μm lasing slope efficiency of Yb, Er:$Ca_2Al_2SiO_7$ crystal due to the addition of Ce co-dopant was reported in Ref. [11], whereas the laser action of Scheelite-like disordered tungstate crystal Yb, Er:$NaGd(WO_4)_2$ does not appear without the addition of high concentrations of Ce [17].

In this paper we studied the spectroscopic properties of another Scheelite-like disordered tungstate crystal $NaLa(WO_4)_2$ (NLW) co-doped by Er and Ce. This group of crystalline hosts is characterized by very large emission probabilities of Re^{3+} ions. Besides that, these hosts give the possibility to insert high concentration of Ce^{3+} [18,19]. NLW possess the tetragonal scheelite-like ($CaWO_4$) structure with space group I41/a [20]. The Er^{3+} and the Ce^{3+} in NLW crystal substitute the La ions. At the range from room temperature up to the melting point NLW have no phase transitions, and, hence, single crystal of this compound can be grown by simple melt growth techniques, in contrast to well-known monoclinic potassium-containing tungstates like $KGd(WO_4)_2$. The smooth contours of the absorption and emission bands of rare earth ions in this group of crystals are due to the disordered structure associated to the random distribution of alkali and rare-earth ions in the Ca^{2+} sublattice. The crystal lattice parameters of NLW are: a=5.325 Å and c=11.701 Å [21].

The complex level configuration of the Er^{3+} ions implies that many processes have to be considered in order to perform the spectroscopic characterization. In order to improve the population inversion, a crucial point is the fast depopulation of the detrimental level $^4I_{11/2}$ through transfer of part of the excited state energy to another rare earth ion. This approach has successfully been tried in the case of Er^{3+} emission at 3 μm and 1.5 μm, using Pr^{3+} [22], Tb^{3+} [23], Eu^{3+} [12] or Ce^{3+} [10,12,16,17,24].

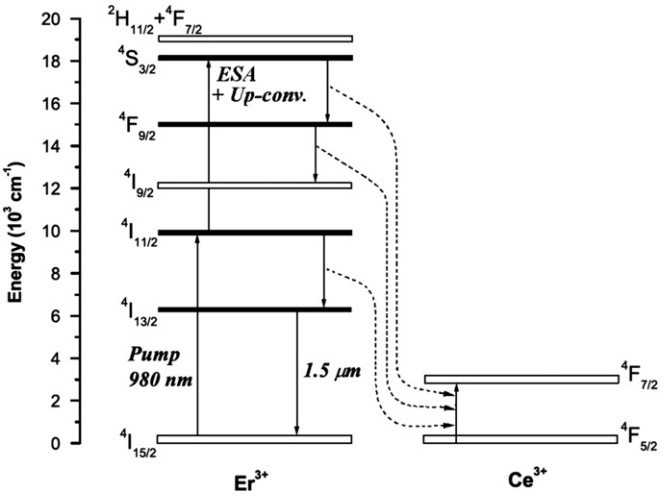

Fig. 1. Scheme of the Er–Ce energy transfer processes.

The advantage of using Ce relies in its energy level scheme that, in the 4f configuration consists of only $^4F_{5/2}$ ground state and the $^4F_{7/2}$ excited state ($\Delta E \approx 3000\ cm^{-1}$).

The energy transfer in Er–Ce codoped system is presented in Fig. 1.

The first effect consists in the increasing of the $^4I_{11/2}\rightarrow{}^4I_{13/2}$ branching ratio through the cross relaxation:

$$^4I_{11/2}(Er),\ ^2F_{5/2}(Ce)\rightarrow{}^4I_{13/2}(Er),\ ^2F_{7/2}(Ce) \quad (1)$$

This effect should result in de-population of the $^4I_{11/2}$ state, and reduction of the pump energy losses for up-conversion to the $^4S_{3/2}$ level. Moreover a direct quenching of $^4S_{3/2}$ by Cerium also exists:

$$^4S_{3/2}(Er),\ ^2F_{5/2}(Ce)\rightarrow{}^4F_{9/2}(Er),\ ^2F_{7/2}(Ce) \quad (2)$$

Furthermore, the energy gap between the $^4F_{9/2}$ and the $^4I_{9/2}$ is reasonable to aspect the following $^4F_{9/2}$ quenching by Cerium:

$$^4F_{9/2}(Er),\ ^2F_{5/2}(Ce)\rightarrow{}^4I_{9/2}(Er),\ ^2F_{7/2}(Ce) \quad (3)$$

Thus, the Ce co-doping produces several quenching processes accumulating the energy in the $^4I_{13/2}$ 1.5 μm emitting level.

2. Experimental

NLW crystals have been grown from stoichiometric melt by the Czochralski method. The growth parameters were: melting temperature ≈1250 °C, growth ambient-air, crucible Pt/Rh, pulling rate at the nominal stage of growth 0.7 mm/h and rotation rate 10 RPM. The single-crystalline bar of undoped NLW cut along *a*-axis, was used as seed. These conditions allowed us to grow the crystals with high optical quality. After growth the crystals were annealed at 700 °C during 3 days. Earlier, for Er, Ce:$NaLa(MoO_4)_2$ crystals the annealing temperature of 1000 °C was applied. However, annealing at this temperature was found to result in turbidity formation of the crystals due to CeO_2 nano-particles precipitation [25]. Reduction of the temperature to 700 °C was found to prevent the turbidity formation for those crystals.

The concentration of Er^{3+} in melt was 1 at% (in respect to total amount of all trivalent cations) for all grown crystals, whereas Ce^{3+} content in the melt was 0, 3, 10 and 20 at% for different crystals. The actual concentration of dopants in our crystals was determined by microprobe analysis at Camebax SX100 analyzer. The average Er concentration appeared to be 0.4 at% or $2.4\times10^{19}\ cm^{-3}$ (i.e. segregation coefficient is evaluated to be about 0.4 [16]). The concentrations of Ce were measured to be 0, 2.2, 7.6 and 16 at%, i.e. the average segregation coefficient of Ce in NLW is 0.75.

In order to investigate the polarization dependent absorption and emission properties, all the crystals are oriented by X-ray backscattering Laue diffractometry and cut along the ***a*** and ***c*** crystallographic axes.

Using a CARY500 spectrophotometer we acquired the room temperature polarized (sigma and pi polarizations corresponding to E II a and E II c respectively) absorption spectra of every sample and, for the single Erbium doped crystal, we performed the same measurement also at T=10 K. The resolutions at room temperature were 1 nm and 0.6 nm for the infrared and the visible regions respectively. At 10 K the resolution has been set to 0.6 nm and 0.3 nm for the infrared and the visible regions.

We recorded the polarized emission spectra around 1.5 μm ($^4I_{13/2}\rightarrow{}^4I_{15/2}$) and around 540 nm ($^4S_{3/2}\rightarrow{}^4I_{15/2}$) at 10, 77 and 300 K. The excitation of samples was provided by a fiber-coupled laser diode emitting around 980 nm with output power of 910 mW. Besides that in some specific cases, discussed below, excitation of the samples at 488 nm with an Ar+ laser was also used.

The emission was collected perpendicular to the incident laser beam to avoid, as much as possible, pump spurious scattering. The luminescence was mechanically chopped and focused by a lens on the input slits of a 320 mm monochromator equipped with different gratings (1200 gr/mm λ_b=500 nm, 600 gr/mm λ_b=1000 nm, 300 gr/mm λ_b=2000 nm) depending on the wavelength range. The emitted radiation was filtered by a Si window for the 1.5 μm measurement. The signal was detected by a S20 cathode photomultiplier for the green region and by a cooled InSb detector in the infrared region, and then processed by a lock-in amplifier. The resolutions of the fluorescence spectra for the infrared and the visible regions were 2.64 nm and 0.66 nm respectively.

For the lifetime measurement of the $^4I_{11/2}$, $^4I_{13/2}$ and $^4S_{3/2}$ multiplets we used a pulsed tunable Ti:Al_2O_3 (Ti:Sa) laser with 10 Hz repetition rate and 30 ns pulse width as excitation source. In the case of direct excitation the $^4S_{3/2}$ level, the Ti:Sa laser was tuned around 800 nm and then frequency doubled by means of a BBO crystal. For these measurements the pulse energy was reduced as much as possible in order to minimize power-dependent effects. Furthermore, to reduce spurious decay-time lengthening produced by radiation trapping, the signal was collected from a small part of the samples (≤ 1 mm^2). The signal was detected by a cooled InSb detector for the infrared emission and by a S20 photomultiplier for the visible region and after appropriate amplification was sent to a digital oscilloscope coupled with a computer. The response time of the system was 1 μs.

3. Results and discussion

3.1. Absorption spectra and Judd–Ofelt analysis

The room temperature polarized absorption spectra of Er:NLW are presented in Fig. 2. In the same figure the assignments of manifolds are given. Within the detection limit of our experimental apparatus, we did not observe any spurious contamination. In the case of the Er, Ce-codoped samples, the spectra were the same as for solely Er-doped NLW except for the presence of the strong broadband absorption of the 4f→5d transition of Ce^{3+} starting from 450 nm [16].

The absorption band near 980 nm, ascribed to the transition $^4I_{15/2}\rightarrow{}^4I_{11/2}$ (Fig. 2 b) is inhomogeneously broadened (due to disorder of the host) with smooth contour. This is convenient from point of view of diode pumping. We calculated from the

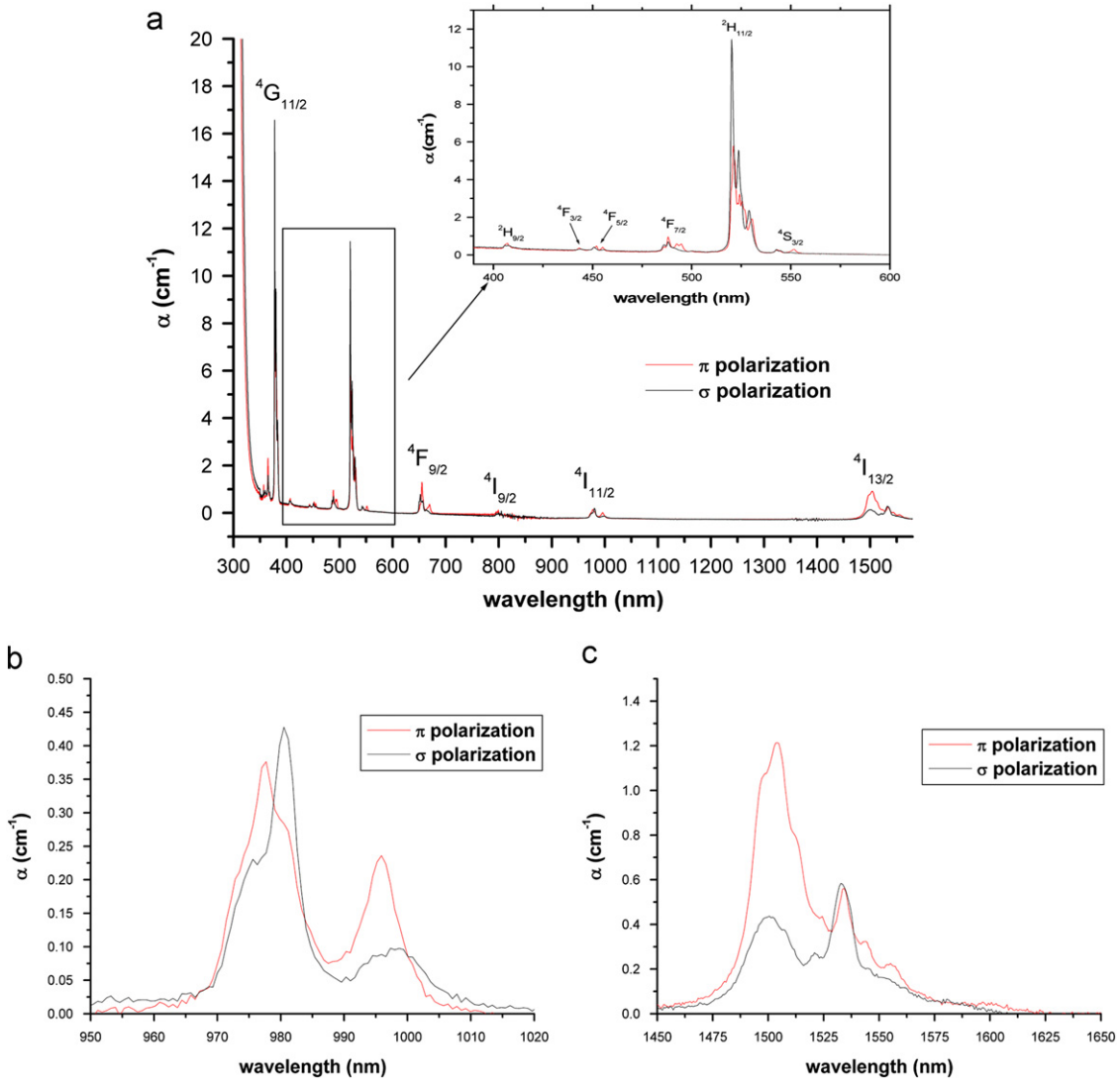

Fig. 2. Polarized absorption spectra of the single Er doped sample at room temperature in the visible (a), 1-μm (b, transition $^4I_{15/2}\rightarrow{}^4I_{11/2}$) and 1.5-μm (c, transition $^4I_{15/2}\rightarrow{}^4I_{13/2}$) spectral ranges.

absorption spectra and the doping concentration, the absorption cross sections: the peak absorption cross-section at $\lambda=981$ nm (σ-polarization) exceeds 1.8×10^{-20} cm^2, which is more than for Er:$YAlO_3$ (0.52×10^{-20} cm^2 [26]), Er:YLF (0.6×10^{-20} cm^2 [27]), and Er:$NaLa(MoO_4)_2$ (1.2×10^{-20} cm^2 [16]) and comparable with that in Er:FAP (1.9×10^{-20} cm^2 [28]).

From the absorption spectra of Er:NLW we calculated the intensity parameters Ω_t ($t=2, 4, 6$) for this crystal using the Judd–Ofelt theory [29,30]. These parameters appeared to be $\Omega_2=6.1$ cm^{-1},$\Omega_4=1.2$ cm^{-1} and $\Omega_6=0.13$ cm^{-1}.

Then the oscillator strengths, spontaneous emission probabilities, and fluorescence branching ratios were calculated. The values of the oscillator strengths are given in Table 1. For the strongest transitions ($^4I_{15/2}\rightarrow{}^4G_{9/2}$, $^4I_{15/2}\rightarrow{}^2H_{11/2}$, $^4I_{15/2}\rightarrow{}^4F_{9/2}$) rather good agreement between the measured and calculated values of oscillator strengths is seen. Unfortunately, for other, weaker transitions the deviation is more essential, so, these values are suitable for estimative calculations only.

The radiative lifetime of the multiplets $\tau_r(J)$ are obtained from the spontaneous emission probabilities $A_{JJ'}$ using the following formula:

$$\tau_r=\frac{1}{\sum_{J'}A_{JJ'}} \tag{4}$$

The calculated radiative lifetimes of the most important manifolds are reported in Table 2.

The obtained values of radiative lifetimes of $^4I_{11/2}$ and $^4I_{13/2}$ states in Er:NLW are rather typical for oxide crystals (for Er:YAG $\tau_{rad}(^4I_{13/2})=8.2$ ms, $\tau_{rad}(^4I_{11/2})=7.5$ ms [31]; for Er:$YAlO_3$ $\tau_{rad}(^4I_{13/2})=3{,}5$ ms, $\tau_{rad}(^4I_{11/2})=7.8$ ms [26]; for Er:KGW $\tau_{rad}(^4I_{13/2})=6.0$ ms, $\tau_{rad}(^4I_{11/2})=5.4$ ms [32];), while the calculated lifetime of $^4S_{3/2}$ is substantially longer than that in most of other crystals. Apparently, this value is overestimated in our case, because of very large (3 times) difference between the calculated and measured oscillator strength for the transition $^4I_{15/2}\rightarrow{}^4S_{3/2}$.

The polarized absorption spectra of the single Er doped sample at 10 K have also been measured. From these spectra the transition energies inside the $NaLa(WO_4)_2$ crystalline host were found.

Table 1
Measured and calculated oscillator strengths for Er:NLW.

Transition	S_{exp} (10^{-21} cm^2)	S_{calc} (10^{-21} cm^2)	Barycenter (nm)
$^4I_{15/2}\rightarrow{}^4I_{13/2}$	3.0	4.4	1522
$^4I_{15/2}\rightarrow{}^4I_{11/2}$	3.3	2.2	983
$^4I_{15/2}\rightarrow{}^4I_{9/2}$	1.0	2.1	801
$^4I_{15/2}\rightarrow{}^4F_{9/2}$	6.6	7.0	657
$^4I_{15/2}\rightarrow{}^4S_{3/2}$	0.9	0.3	546
$^4I_{15/2}\rightarrow{}^2H_{11/2}$	45.1	48.5	523
$^4I_{15/2}\rightarrow{}^4F_{7/2}$	3.7	2.6	490
$^4I_{15/2}\rightarrow{}^4F_{5/2}+{}^4F_{3/2}$	1.4	0.4	450
$^4I_{15/2}\rightarrow{}^4G_{9/2}$	1.2	0.5	408
$^4I_{15/2}\rightarrow{}^4G_{11/2}$	65.1	62.5	380
$^4I_{15/2}\rightarrow{}^4G_{9/2}+{}^2K_{15/2}$	6.7	4.9	364

Table 2
Calculated radiative lifetimes for the manifolds under investigation.

Manifold	T_r (msec)
$^4I_{13/2}$	6.19
$^4I_{11/2}$	5.86
$^4S_{3/2}$	2.14

3.2. Fluorescence spectra and lifetime measurements

3.2.1. Cryogenic emission spectra and Stark sub-levels positions

We acquired the Er:NLW emission spectra at 10 K and at 77 K (Fig. 3).

These measurements allowed us to observe the energy positions of Stark sub-levels for the ground state and to perform a further check for the excited manifolds. The measured values are presented in Table 3.

It is seen from Table 3 that Stark splitting of Er ground state in Er:NLW crystal is 295 cm^{-1}. This value is typical for Erbium in double tungstate crystals (361 cm^{-1} for Er:KGW [32]; 313 cm^{-1} for Er:$NaBi(WO_4)_2$ [33]), and it is not very high in comparison with oxide crystals of other families (568 cm^{-1} for Er:YAG [34]; 552 cm^{-1} for Er:$YAlO_3$ [26]), although, higher than that in halogenide crystals (240 cm^{-1} for Er:KPb_2Cl_5 [35]). So, due to three-level scheme of Er 1.5-μm laser operation one can expect rather essential thermal population of upper Stark sub-levels of Er ground state in Er:NLW crystal. Therefore, the optimal (not very high) Erbium concentration, and control of thermal loading of the active medium are very important for low threshold laser operation at Er:NLW crystal.

It is also seen from Table 3 that for some manifolds the number of observed Stark sub-levels exceeds the theoretically possible one. It can be explained by the following reasons: distribution of Na and Ln ions over dodecahedral site 4a in the structure of scheelite-like double tungstates is, in fact, not completely random. Some partial ordering in that distribution do exist. This leads to splitting of 4a site into two different subkinds of dodecahedral sites with local symmetries 2b and 2d. The overall space group of the crystal decreases in this case from $I4_1/a$ to I/4. This effect was described for the first time in scheelite-like tungstate crystal $NaBi(WO_4)_2$ [36] and confirmed later for another crystal of this family Tm:$NaGd(WO_4)_2$ [37]. The same effect occurs, apparently, in NLW as well, although we failed to find the appropriate investigations for this crystal in the available literature, and have not performed the corresponding studies by ourselves to the moment.

Erbium ions enter into both 2b and 2d sub-sites, and have there slightly different Stark splitting of its manifolds. This results in appearance of the additional peaks at both the absorption and the emission spectra at 10 K. Similar situation was observed earlier for Erbium doped yttrium stabilized zirconia (YSZ) single crystals [38].

3.2.2. Room-temperature emission spectra

In Fig. 4 the polarized emission spectra for the Er:NLW crystal at room temperature, in the green and 1.5 μm regions are presented.

In these spectral regions there are three distinguishable bands around 531, 552 and 1535 nm, corresponding to the $^2H_{11/2}\rightarrow{}^4I_{15/2}$, $^4S_{3/2}\rightarrow{}^4I_{15/2}$ and $^4I_{13/2}\rightarrow{}^4I_{15/2}$ transitions, respectively. Using well-known Füchtbauer–Landeburg equation [39] we evaluated the peak fluorescence cross-sections for the $^4I_{13/2}\rightarrow{}^4I_{15/2}$ transition. The cross-sections are 5.7×10^{-21} cm^2 for π polarization ($\lambda_{max}=1506$ nm), and 5.2×10^{-21} cm^2 for σ polarization ($\lambda_{max}=1535$ nm). This is comparable with that for another scheelite-like crystal Er:$NaBi(WO_4)_2$ (5×10^{-21} cm^2 [40]), as well as for Er:YAG (6.6×10^{-21} cm^2 [31]), and Er:YLF (5.5×10^{-21} cm^2 [41]), although it is several times less than for Er:YVO_4 [42,43] or for Er-doped monoclinic tungstates [44]. The fluorescence cross-sections at $\lambda\sim1600$ nm (where low-threshold laser action can be reached due to the absence of significant absorption) are about 2×10^{-21} cm^2 for both polarizations.

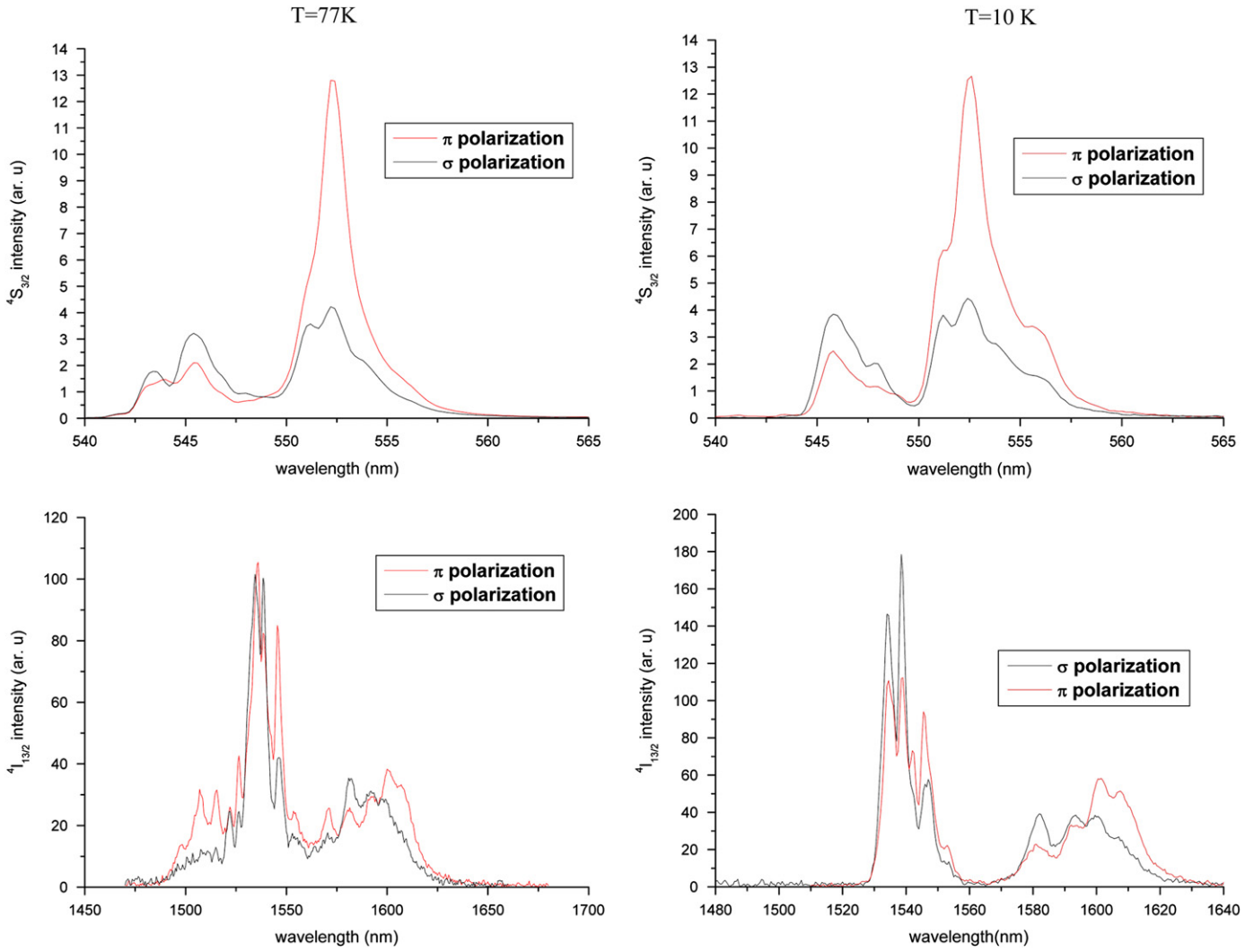

Fig. 3. Polarized emission spectra of the single Er doped sample at 10 K and 77 K.

Table 3
Energies transitions observed from the low temperature measurement.

$^{2S+1}L_J$	Observed energy levels (cm^{-1})	Number of observed levels
$^4I_{15/2}$	0, 25, 57, 100, 218, 250, 264, 277, 295	9
$^4I_{13/2}$	6507, 6526, 6533, 6559, 6577, 6643, 6688	7
$^4I_{11/2}$	10,200, 10,216, 10,231, 10,254, 10,290, 10,298	6
$^4I_{9/2}$	12,366, 12,434, 12,453, 12,508, 12,530, 12,596	6
$^4F_{9/2}$	15,240, 15,272, 15,291, 15,335, 15,352, 15,406	6
$^4S_{3/2}$	18,353, 18,372, 18,440, 18,484	4
$^2H_{11/2}$	19,081, 19,098, 19,111, 19,156, 19,205, 19,242	6
$^4F_{7/2}$	20,464, 20,493, 20,511, 20,589, 20,607	5
$^4F_{5/2}+^4F_{3/2}$	22,190, 22,229, 22,581	3
$^2H_{9/2}$	24,496, 24,557, 24,596, 24,631, 24,648, 24,680	6
$^4G_{11/2}$	26,318, 26,368, 26,433, 26,496	4
$^2G_{9/2}+^2K_{15/2}$	27,370, 27,416, 27,432, 27,504, 28,051	5

3.2.3. *Lifetimes measurements*

For the single doped Er:NLW sample we acquired the lifetimes of the $^4S_{3/2}$, $^4I_{11/2}$ and $^4I_{13/2}$ multiplets at different temperatures from 10 K to 300 K. The lifetimes for each level as a function of the temperature are shown in Fig. 5. It is seen that in all studied cases the variation of measured lifetime values does not exceed 20%. The reduction of fluorescence lifetimes with increase in the temperature is, apparently, due to the multiphonon non-radiative relaxation. Following the phenomenological model of Riseberg–Moos [45] the temperature dependence of the multiphonon relaxation rate is given by:

$$\tau_{ph}^{-1}(T) = \tau_{ph}^{-1}(0)(1+n)^p \quad (5)$$

$$n = 1/[\exp(h\omega/kT) - 1] \quad (6)$$

where $h\omega$ is energy of the phonon participating in the relaxation process, p is the number of phonons required for bridging the energy difference between the relaxating state and the next (lower) electronic level. This energy difference is at least on the order of $\sim 3000\ cm^{-1}$. The maximum phonon energy of the (WO_4) group is about $900\ cm^{-1}$ [46], i.e. several times larger than kT at room temperature. It means that the value of n will be much less than 1 in Er:NLW crystal even at 300 K, whereas the value of p exceeds 3 at this temperature.

Thus, the non-radiative relaxation rates of $^4S_{3/2}$, $^4I_{11/2}$ and $^4I_{13/2}$ manifolds (and, hence, measured lifetimes) should not be very high at 300 K, and should be very slightly sensitive to the temperature within the range 0–300 K. Just this situation is observed in Fig. 5. Similar dependencies are typical also for Er ion in other tungstate crystals Er:KGW [32] and Er:KYW [46], although in Er:YVO [48] and Er:YSZ [38] the dependence of τ_{ph} from temperature is rather significant, possibly, due to substantially less $h\omega$.

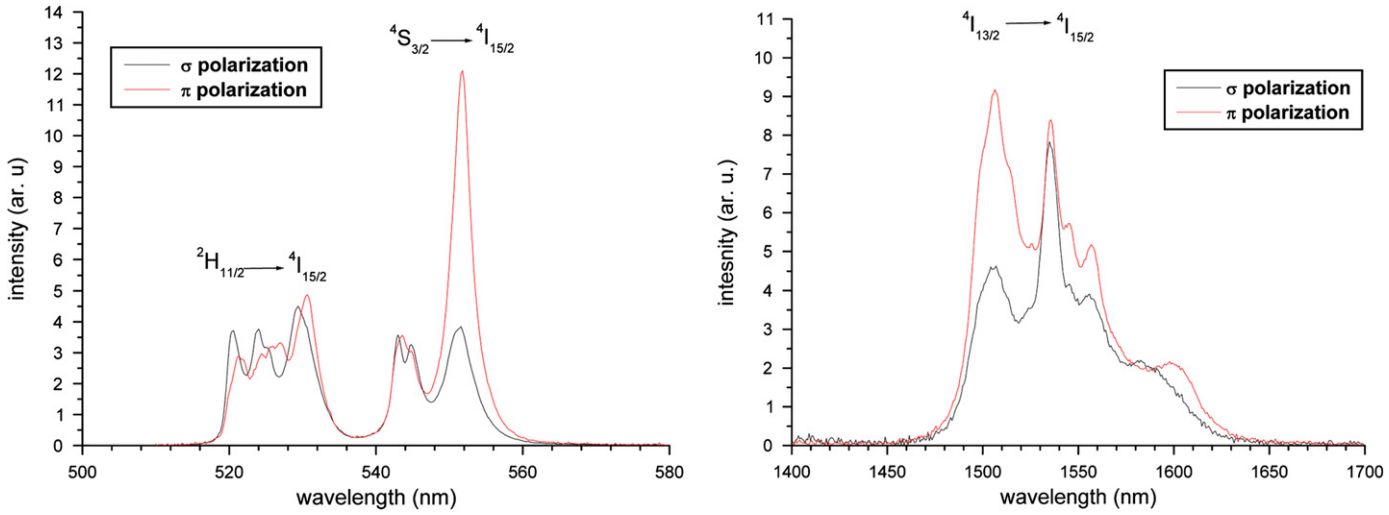

Fig. 4. Polarized emission spectra of the single Er doped sample at room temperature.

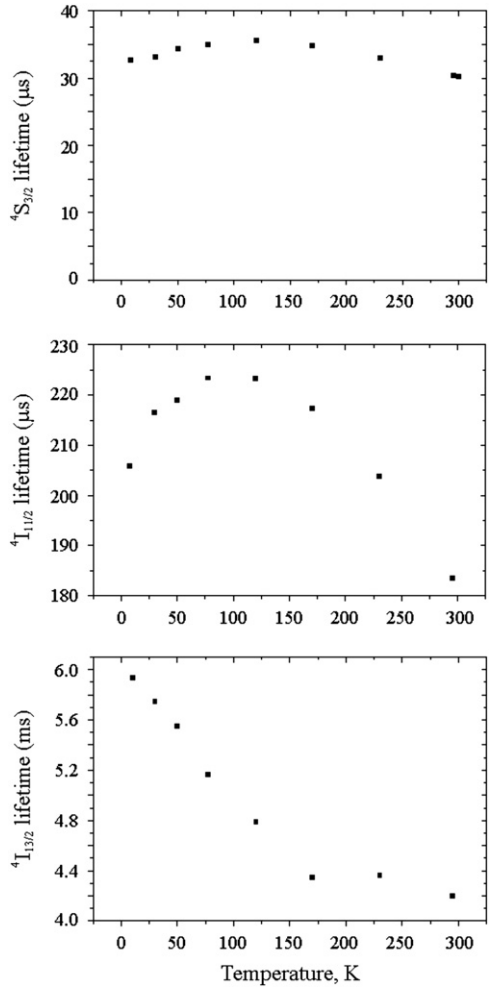

Fig. 5. Lifetimes of the $^4S_{3/2}$, $^4I_{11/2}$ and $^4I_{13/2}$ manifolds of Er:NLW crystal at different temperatures.

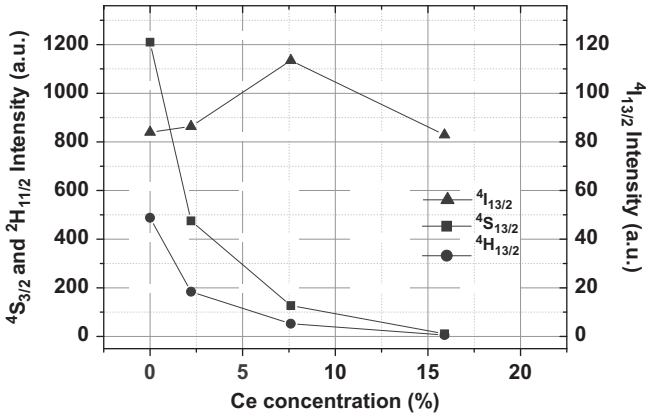

Fig. 6. Intensity of the emission from $^2H_{11/2}$, $^4S_{3/2}$ and $^4I_{13/2}$ levels to the ground state $^4I_{15/2}$, as function of the Ce concentration at room temperature.

The lifetime of $^4I_{13/2}$ at 10 K is close to the calculated radiative lifetime (see Table 2). At heating the crystal it slightly decreases until 170 K and after that becomes quite constant. Meanwhile, the measured lifetimes of $^4S_{3/2}$ and $^4I_{11/2}$ are very far from the calculated radiative lifetimes (even with taking into account the probable overestimation of the value of $^4S_{3/2}$ radiative lifetime by Judd–Ofelt analysis, see above). Such deviations are rather typical for Erbium doped dielectric crystals (for Er:YAG $\tau_{rad}(^4S_{3/2})=450\,\mu s$ at 300 K [49], whereas $\tau_{meas}(^4S_{3/2})=16.7\,\mu s$ [50]; $\tau_{rad}(^4I_{11/2})=7.5$ ms [31], whereas $\tau_{meas}(^4I_{11/2})=100\,\mu s$ [50]; for Er:KGW $\tau_{rad}(^4S_{3/2})=758\,\mu s$, $\tau_{meas}(^4S_{3/2})=27\,\mu s$; $\tau_{rad}(^4I_{11/2})=5.4$ ms, $\tau_{meas}(^4I_{11/2})=158\,\mu s$ [32]). This fact is usually explained by very large value $\tau_{ph}^{-1}(0)$ for $^4S_{3/2}$ and $^4I_{11/2}$ states [32,42].

From Fig. 5 it is also seen that measured lifetimes of both $I_{11/2}$ and $^4S_{3/2}$ slightly increase up to the temperature of about 120 K. This fact is not observed for any Er-doped crystal in the available literature. It can, probably, be explained by large fluorescence reabsorption at very low temperatures, when only the lowest Stark sublevels of $^4I_{11/2}$ and $^4I_{15/2}$ are populated, and only resonant transitions occur. For higher temperatures the resonance in absorption and emission destroys, since other sublevels also become populated.

3.2.4. Ce influence on the emission properties

The trends of fluorescence intensity for the $^2H_{11/2} \rightarrow {}^4I_{15/2}$, $^4S_{3/2} \rightarrow {}^4I_{15/2}$ and $^4I_{13/2} \rightarrow {}^4I_{15/2}$ transitions with increase of Cerium content in crystals are presented in Fig. 6 (pumping was performed at 980 nm), the fluorescence intensities were measured at 531, 552 and 1535 nm, respectively. Decrease the intensities of

transitions $^2H_{11/2}\rightarrow{}^4I_{15/2}$ and $^4S_{3/2}\rightarrow{}^4I_{15/2}$ is accompanied by increase of $^4I_{13/2}\rightarrow{}^4I_{15/2}$ transition intensity except for the sample doped by 16 at% Ce.

In case of pumping the crystal at 980 nm, the levels $^4S_{3/2}$ and $^2H_{11/2}$ are excited by up-conversion and ESA processes through $^4I_{11/2}$ manifold (see Fig. 1). Therefore, decrease of the green emission intensity with increase of Cerium doping level can be caused by direct quenching of $^4S_{3/2}$ ($^2H_{11/2}$) by Cerium (see Eq. (2)), and/or by the reduction of population the $^4I_{11/2}$ manifold (see Eq. (2)) and, hence, by worsening of $^4S_{3/2}$ ($^2H_{11/2}$) feeding from this manifold.

For revealing the further transformation of the excited state energy from the $^4S_{3/2}$ level, we studied the quenching of $^4S_{3/2}$ green fluorescence by Ce^{3+} ion according to scheme (2).

We measured the $^4S_{3/2}$ decay kinetics with excitation in the crystals by short ($\Delta t\sim20$ nsec) pulses of the second harmonic of Nd:YAG laser (532 nm) into the $^2H_{11/2}$ level of erbium. This excitation can be considered as practically the direct pumping of $^4S_{3/2}$ manifold because of very strong phonon coupling of $^2H_{11/2}$ and $^4S_{3/2}$ multiplets. The fluorescence from $^4S_{3/2}$ level was registered at $\lambda\sim850$ nm (transition $^4S_{3/2}\rightarrow{}^4I_{13/2}$). The signal from the photomultiplier was transferred into the digital oscilloscope. The temporal resolution of this system was not longer than 1 μsec.

The decay curves of $^4S_{3/2}\rightarrow{}^4I_{13/2}$ emission for different Ce^{3+} concentrations are presented in Fig. 7. In the crystal without Ce the decay time is 30 μsec. In the Ce-codoped crystals the decay curves become nonexponential, since each of many variants of Er–Ce arrangements with different distances has its own probability of interaction. At the beginning parts of the decay curves the lifetimes are: 11.5 μsec (2.2% Ce), 6.5 μsec (7.6% Ce) and 2.5 μsec (15.9% Ce). Based on these lifetimes we evaluated the parameter of donor–acceptor interaction C_{DA}, which is equal to the probability of the interaction W_{DA} in the case when the distance between donor and acceptor is equal to 1 cm. It is well known that for dipole–dipole interaction, which is the main mechanism for our case, $W_{DA}=C_{DA}/R^6$. The C_{DA} parameter is calculated based both on experimental values, and on calculation of the lattice sum [26,27]:

$$W = x_A C_{DA} \sum \frac{1}{R_i^6} \tag{7}$$

where x_A is the arbitrary concentration of acceptors, W is the experimental decay rate on the initial stage, $\Sigma\left(1/R_i{}^6\right)$ is the lattice sum, calculated from the crystallographic data. We calculated the lattice sum $\Sigma(1/R_i^6)$, based on the 6 nearest distances between the cation positions, occupied by rare-earth ions (these distances can be easily derived from the structural data of the crystal). The calculated lattice sum is $\sim7\times10^{44}\mathrm{cm}^{-6}$, and the value of C_{DA} appeared to be $\sim3\times10^{-39}\,\mathrm{cm}^6\,\mathrm{sec}^{-1}$.

These results allow to determine the reduction of the intensity of green Er^{3+} fluorescence (transition $^4S_{3/2}\rightarrow{}^4I_{15/2}$) due to the direct quenching of the Er^{3+} level $^4S_{3/2}$ by Ce^{3+}, and, thus, to separate the contribution of this mechanism from the reduction of the green fluorescence intensity due to diminishing of the population of $^4I_{11/2}$ and, hence, due to decrease of the up-conversion feeding the $^4S_{3/2}$ excited state. In fact, the ratio of intensities of the fluorescence from $^4S_{3/2}$ in case of direct steady excitation for the samples with different Ce concentrations are equal to the ratios of the squares under the decay curves, presented in Fig. 7: $I_{0\%\ Ce}$: $I_{2.2\%\ Ce}$: $I_{7.6\%\ Ce}$: $I_{15.9\%\ Ce}$= 1:0.73:0.35:0.13. (here $I_{0\%\ Ce}$ is assumed to be 1). Since the intensity of green luminescence decreases with increase of Ce concentration more quickly, than the demonstrated by these ratios (compare with Fig. 6), we came to the conclusion, that both of mentioned above processes give substantial contribution in total reduction of population of the $^4S_{3/2}$ level.

Note, that C_{DA} value for the process (2) are nearly the same for the tungstate and molybdate crystals. Therefore, the efficiency of quenching of luminescence from the $^4S_{3/2}$ by Ce^{3+} ions in these crystals are close to each other for equal cerium concentrations.

In order to characterize quantitatively the quenching of luminescence from $^4I_{11/2}$ state, we measured the luminescence decay curves from this level by method, described above for the level $^4S_{3/2}$. The luminescence signal was measured at 998 nm. In the crystals, without Ce content the decay time is 183 μsec (Fig. 8). In Ce-codoped crystals the decay curves become non-exponential. Since the excitation was not resonance, the initial luminescence rising appeared (not shown in Fig. 8). For the decay curve of the most heavily Ce codoped sample, where such a rising was the shortest, τ at initial stage is ≈9.5 μs. From these data the C_{DA} estimation from below for dipole–dipole interaction for the process (1) gives: $C_{DA}\geq9\times10^{-40}\,\mathrm{cm}^6\,\mathrm{sec}^{-1}$. The same measurements made on Er, Ce:$NaLa(MoO_4)_2$ crystal gave the equal value, the calculations of the interaction microparameter using the data of Ref. [16] gave the value $C_{DA}\approx10\times10^{-40}\,\mathrm{cm}^6\,\mathrm{sec}^{-1}$ for Er, Ce:$NaLa(MoO_4)_2$ crystal. Based on these data the efficiency of luminescence quenching from $^4I_{11/2}$ level by Cerium ions at equal Ce^{3+} concentrations should be approximately the same for both tungstate and molybdate crystals.

The measured average lifetimes of the $^4S_{3/2}$, $^4I_{11/2}$ and $^4I_{13/2}$ multiplets of Er, Ce:NLW crystals as a function of Cerium concentration at room temperature are presented in Fig. 9.

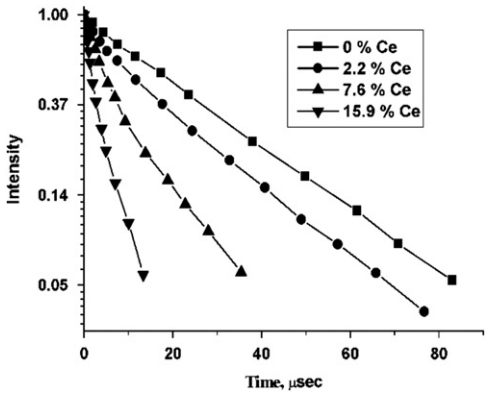

Fig. 7. The decay curves of $^4S_{3/2}\rightarrow{}^4I_{13/2}$ emission for the different Ce^{3+} concentrations.

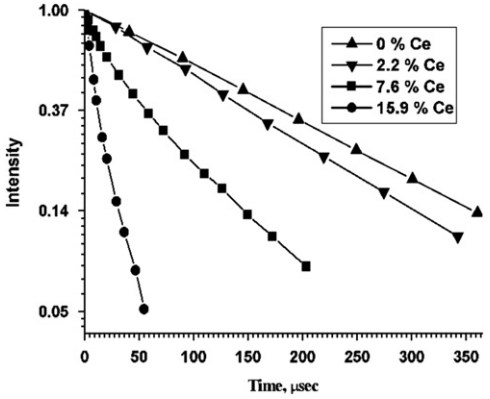

Fig. 8. The decay curves of $^4I_{11/2}\rightarrow{}^4I_{15/2}$ emission for the different Ce^{3+} concentrations.

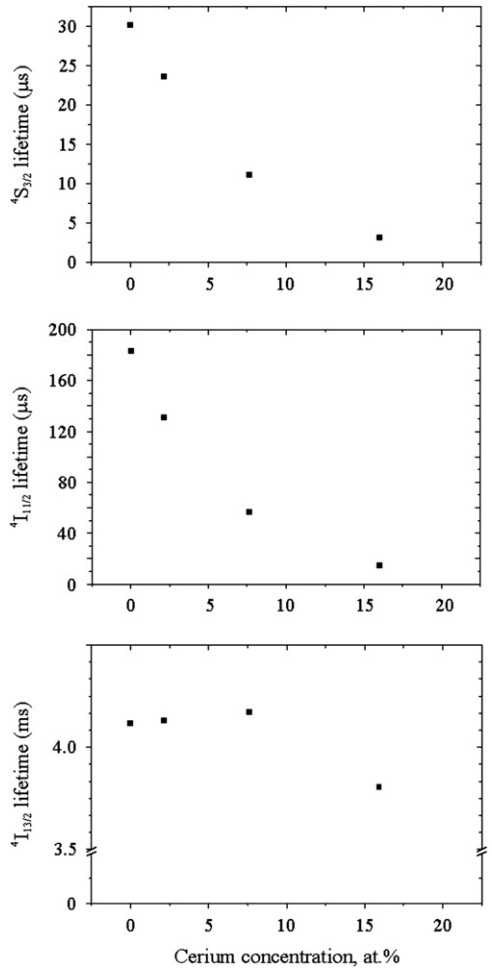

Fig. 9. Lifetimes of the $^4S_{3/2}$, $^4I_{11/2}$ and $^4I_{13/2}$ manifolds of Er, Ce:NLW crystals as a function of Cerium concentration.

It is seen, that reduction of the $^4I_{13/2}$ lifetime can be observed only for the crystal containing 15.9 at% of Ce, and the value of this reduction is only about 10% in respect to the single Er doped crystal. This effect, as well as the slight reduction of 1.5 μm emission intensity (see Fig. 5) is, apparently, caused by some quenching of $^4I_{13/2}$ manifold by Cerium in case of very big concentrations of Ce^{3+} in the crystals. It is noted also, that the quenching of $^4I_{13/2}$ lifetime with addition of 20 at% Ce to Er:NLM crystal was as large as ~15% (versus ~10% in NLW:Er, Ce).

4. Conclusion

We performed a spectroscopic investigation of the NLW crystalline host doped with 0.4 at% of Er^{3+}. The Judd–Ofelt parameters are calculated using the absorption spectra of the crystal. Using the low temperature absorption spectra we presented here for the first time the values of the energy levels for Erbium ions in the $NaLa(WO_4)_2$ crystal.

Since the reduction of the $^4I_{11/2}$ and $^4S_{3/2}$ fluorescence intensities and measured lifetimes with the increase of the Ce concentration we demonstrated that the Ce presence can help the population inversion efficiency for the 1.5 μm emission without substantially affecting the $^4I_{13/2}$ lifetime. Thus, the Er,Cr:NLW crystal is a very promising material for obtaining a low-thereshold 1.5 μm laser action. The lasing experiments at this crystal will be performed in the near future.

Acknowledgments

Authors are grateful to I. Grassini of Pisa University for her contribution in the sample preparation. This work has been supported by RFBR (Grant ♯ 09-02-92434-KE_a).

References

[1] H.-L. Xu, Z.-K. Jiang, Chem. Phys. 287 (2003) 155.
[2] A. Silversmith, J. Lumin. 60–61 (1994) 363.
[3] M.-C. Pujol, M. Rico, C. Zaldo, R. Sole, V. Nikolov, X. Solans, M. Aguilio, F. Diaz, Appl. Phys. B 68 (1999) 187.
[4] Q. Wang, N.-K. Dutta, R. Ahrens, J. Appl. Phys. 95 (2004) 4025.
[5] R. Guo, Y.-C. Wu, P.-Z. Fu, F.-L. Jing, Chem. Phys. Lett. 461 (2005) 133.
[6] Springer Handbook of Lasers and Optics, Frank Träger (Ed.), 1310 p., 2007.
[7] C. Li, R. Moncorge, J.C. Sourieau, C. Borel, C. Wyon, Opt. Commun. 107 (1994) 61.
[8] T. Schweizer, T. Jensen, E. Heumann, G. Huber, Opt. Commun. 118 (1995) 557.
[9] S.B. Stevens, C.A. Morrison, T.H. Allik, A.L. Rheingold, B.S. Haggerty, Phys. Rev. B 43 (1991) 7386.
[10] B. Simondi-Teisseire, B. Viana, A.-M. Lejus, J.-M. Benitez, D. Vivien, C. Borel, R. Templier, C. Wyon, IEEE J. Quantum Electron. 32 (1996) 2004.
[11] A. Braund, S. Girard, J.L. Doualan, M. Thuau, R. Moncorge, A.M. Tkachuk, Phys. Rev. B 61 (2000) 5280.
[12] Y.-G. Choi, K.-H. Kim, S.-H. Park, J.J. Heo, Appl. Phys. 88 (2000) 3832.
[13] Z. Meng, T. Yoshimura, K. Fukue, M. Higashihata, Y. Nakata, T.J. Okada, Appl. Phys. 88 (2000) 2187.
[14] C. Strohofer, A. Polman, Opt. Mater. 17 (2001) 445.
[15] E. Sani, A. Toncelli, M. Tonelli, Opt. Express 13 (22) (2005) 8980.
[16] E. Sani, A. Toncelli, M. Tonelli, D.A. Lis, E.V. Zharikov, K.A. Subbotin, V.A.J. Smirnov, Appl. Phys. 97 (2005) 123531.
[17] J. Huang, Y. Chen, Y. Lin, X. Gong, Z. Luo, Y. Huang, Opt. lett. 33 (21) (2008) 2548.
[18] Yu.-K. Voron'ko, E.-V. Zharikov, D.-A. Lis, A.A. Sobol', K.A. Subbotin, S.N. Ushakov, V.E. Shukshin, Inorg. Mater. 39 (2003) 1308.
[19] Yu.-K. Voron'ko, E.-V. Zharikov, D.-A. Lis, A.A. Sobol', K.A. Subbotin, S.N. Ushakov, V.E. Shukshin, Proc. SPIE 5478 (2004) 60.
[20] V.K. Trunov, V.A. Efremov, A. Velikodnyi Yu, Crystallochemistry and Properties of Double Molybdates and Tungstates, Nauka, Leningrad, 1986, p. 176, (in Russian).
[21] K. Byrappa, A.J. Jain, Mater. Res. 11 (1996) 2869.
[22] D.-S. Knowles, H.-P. Jenssen, IEEE J. Quantum Elect. 28 (1992) 1197.
[23] A.A. Andronov, I.A. Grishin, V.A. Gur'ev, V.V. Orekhovski, A.P. Savikin, Tech. Phys. Lett. 24 (1998) 365.
[24] X. Wang, Q. Nie, T. Xu, S. Dai, X. Shen, L. Liu. J. Opt. Soc. Am. B 24 (4) 972.
[25] E.I. Suvorova, G.M. Kuz'micheva, A.V. Morozkin, E.V. Zharikov, D.A. Lis, K.A. Subbotin, Inorg. Mater. 43 (3) (2007) 287.
[26] D.K. Sardar, S. Chandrasekharan, K.L. Nash, J.B. Gruber, J. Appl. Phys. 104 (2008) 023102-1-8.
[27] P.E.-A. Möbert, E. Heumann, G. Huber, B.H.T. Chai, Opt. Lett. 22 (18) (1997) 1412.
[28] D.K. Sardar, C.H. Coeckelenbergh, R.M. Yow, J.B. Gruber, T.H. Allik, J. Appl. Phys. 98 (2005) 033535-1-7.
[29] R. Judd, Phys. Rev. 127 (1962) 750.
[30] G.S.J. Ofelt, Chem. Phys. 37 (1962) 511.
[31] J.O. White, M. Dubinskii, L.D. Merkle, I. Kudryashov, D. Garbuzov, J. Opt. Soc. Am. B 24 (9) (2007) 2454.
[32] M.C. Pujol, M. Rico, C. Zaldo, R. Sole, V. Nikolov, X. Solans, M. Aguilo, F. Dıaz, Appl. Phys. B 68 (1999) 187.
[33] M. Rico, V. Volkov, C. Cascales, C. Zaldo, Chem. Phys. 279 (2002) 73.
[34] K. Spariosu, M. Birnbaum, B. Viana, J. Opt. Soc. Am. B 11 (5) (1994) 894.
[35] J.B. Gruber, R.M. Yow, A.S. Nijjar, C.C. Russell, D.K. Sardar, B. Zandi, A. Burger, U.N. Roy, J. Appl. Phys. 100 (2006) 043108.
[36] C. Cascales, M.D. Serrano, F. Esteban-Betegon, C. Zaldo, Phys. Rev. B 74 (2006) 174114-1.
[37] F.A. Bolschikov, G.M. Kuz'micheva, D.A. Lis, Yu.M. Papin, A.V. Popov, P.A. Ryabochkina, V.B. Rybakov, V.G. Senin, V.A. Smirnov, K.A. Subbotin, Yu K. Voron'ko, V.V. Voronov, E.V. Zharikov, J. Cryst. Growth 311 (17) (2009) 4171.
[38] R.I. Merino, V.M. Orera, R. Cases, M.A. Chamarro, J. Phys. Condens. Matt. 3 (1991) 8491.
[39] B.M. Walsh, N.P. Barnes, B. Di Bartolo, J. Appl. Phys. 83 (5) (1998) 2772; T.S. Kubo, T.J. Kane, IEEE J. Quantum Electron. 28 (1992) 1033.
[40] M. Rico, A. Mendez-Blas, V. Volkov, M.A. Monge, C. Cascales, C. Zaldo, A. Kling, M.T. Fernandez-Diaz, J. Opt. Soc. Am. B 23 (10) (2006) 2066.
[41] A. Diening, E. Heumann, G. Huber, O. Kuzmin, Tech. Digest Ser. 6 (1998) 299.
[42] S. Golab, P. Solarz, G. Dominiak-Dzik, T. Lukasiewicz, W. Ryba-Romanowski, J. Alloy. Compd. 341 (2002) 165.
[43] I. Sokolska, E. Heumann, S. Kuck, T. Łukasiewicz, Appl. Phys. B 71 (2000) 893.
[44] X. Mateos, R. Solé, Jna Gavaldà, M. Aguiló, J. Massons, F. Díaz, Opt. Mater. 28 (4) (2006) 423.

[45] L.A. Riseberg, H.W. Moos, Phys. Rev. 174 (1968) 429.
[46] L. Macalik, J. Hanuza, A.A. Kaminskii, J. Mol. Struct. 555 (2000) 289.
[48] S. Golab, W. Ryba-Romanowski, G. Dominiak-Dzik, T. Lukasiewicz, M. Swirkowicz, J. Alloy. Compd. 323–324 (2001) 288.
[49] D.K. Sardar, W.M. Bradley, J.J. Perez, J.B. Gruber, B. Zandi, J.A. Hutchinson, C. Ward, M.R. Kokta, J. Appl. Phys. 93 (5) (2003) 2602.
[50] S. Georgescu, O. Toma, C. Florea, C. Naud., J. Lumin. 101 (2003) 87.